J Pharmacol Sci 103, 159 – 167 (2007)

Journal of Pharmacological Sciences

Full Paper

Caspase Cascade Proceeds Rapidly After Cytochrome *c* Release From Mitochondria in Tumor Necrosis Factor-α-Induced Cell Death

Hiroshi Kawai[1,3,*], Takuo Suzuki[1], Tetsu Kobayashi[1], Akiko Ishii-Watabe[1], Haruna Sakurai[2], Hisayuki Ohata[2], Kazuo Honda[2], Kazutaka Momose[2], Takao Hayakawa[1], and Toru Kawanishi[1,#]

[1]*Division of Biological Chemistry and Biologicals, National Institute of Health Sciences, Tokyo 158-8501, Japan*
[2]*Department of Pharmacology, School of Pharmaceutical Sciences, Showa University, Tokyo 142-8555, Japan*
[3]*Faculty of Pharmaceutical Sciences, Josai International University, Chiba 283-8555, Japan*

Received August 2, 2006; Accepted December 2, 2006

Abstract. The caspase activation cascade and mitochondrial changes are major biochemical reactions in the apoptotic cell death machinery. We attempted to clarify the temporal relationship between caspase activation, cytochrome *c* release, mitochondrial depolarization, and morphological changes that take place during tumor necrosis factor (TNF)-α-induced cell death in HeLa cells. These reactions were analyzed at the single-cell level with 0.5 – 1 min resolution by using green fluorescent protein (GFP)-variant-derived probes and chemical probes. Cytochrome *c* release, caspase activation, and cellular shrinkage were always observed in this order within 10 min in all dying cells. This sequence of events was thus considered a critical pathway of cell death. Mitochondrial depolarization was also observed in all dying cells observed, but frequently occurred after caspase activation and cellular shrinkage. Mitochondrial depolarization is therefore likely to be a reaction that does not induce caspase activation and subsequent cellular shrinkage. Mitochondrial changes are important for apoptotic cell death; moreover, cytochrome *c* release, and not depolarization, is a key reaction related to cell death. In addition, we also found that the apoptotic pathway proceeds only when cells are exposed to TNF-α. These findings suggest that the entire cell death process proceeds rapidly during TNF-α exposure.

Keywords: tumor necrosis factor (TNF)-α, cytochrome *c*, mitochondrial depolarization, caspase, real-time imaging

Introduction

Apoptosis is a mechanism of cell death that is mediated by various intracellular reactions. A family of cysteine proteases, the caspases, forms the activation cascade, and these proteases play a central role in the apoptotic cell death machinery (1, 2). The caspases usually exist as pro-proteins in living cells and are activated by cleavage at the time when cell death is induced. In an early phase of the cell death process, initiator caspases are activated, which in turn activate effector caspases (3 – 7). Activated effector caspases cleave a number of different target proteins, and this cleavage leads ultimately to apoptotic cell death (8, 9). Mitochondria also play an important role in the cell death process (10 – 13). Cellular stresses induce mitochondrial changes, including an increase in outer mitochondrial membrane permeability; various mitochondrial proteins such as cytochrome *c* (cyt.*c*) and second mitochondrial activator of caspases (Smac) are released into the cytosol. Released proteins directly or indirectly regulate caspase activation and/or other reactions, which eventually induce cell death.

Various factors in the cell death process have been identified, but correlation among these factors remains unclear. Cell death events such as caspase activation and mitochondrial changes are rapid processes, and the onset of these events varies between individual cells (14 – 17). So, it is difficult to determine how and when such

*Corresponding author (affiliation #3). hkawai@jiu.ac.jp
#Present affiliation: Division of Drugs, National Institute of Health Sciences, Tokyo 158-8501, Japan
Published online in J-STAGE: February 8, 2007
doi: 10.1254/jphs.FP0060877

reactions occur in cells as based on analyses of cell populations, which can only be used to detect an average value for a large number of individual cells. In order to gain a better understanding of the cell death mechanism, simultaneous multi-events analyses should be conducted at the single-cell level and with high spatial and temporal resolution. Real-time imaging with confocal microscopy is a powerful method of detecting the manner in which such rapid intracellular reactions take place (18, 19).

Fluorescence resonance energy transfer (FRET) is useful for imaging analyses. Variants of green fluorescent protein (GFP) are currently widely employed; several families of fluorescent proteins have recently been reported to be useful for FRET analysis (19 – 22). Previously, we developed genetically-encoded sensors for caspase activation that consist of two fluorescent proteins linked by a small peptide (23, 24). Cyan-, green-, yellow-, and red-fluorescent proteins (CFP, GFP, YFP, DsRed) were used in combination as the fluorescent proteins. The small peptide was derived from a substrate of caspase, poly(ADP-ribose)polymerase; this fusion protein was primarily cleaved by caspase 3 (23). The sensor protein exhibits FRET in its intact form. However, in the presence of active caspase, the peptide is cleaved, and the two fluorescent proteins are rendered far apart; in this case, the sensor protein no longer exhibits any FRET. Caspase activation is detected as a reduction in FRET. We have previously reported that the use of various color combinations facilitates real-time imaging analysis. In particular, GFP-DsRed and YFP-DsRed have been shown to be as sensitive as CFP-YFP, which is commonly used as the FRET pair. FRET probes that consist of such color variations may be useful for simultaneous multi-event imaging (24).

In this study, we used the YFP-DsRed version of the effector-caspase sensor (YRec), CFP-tagged cyt.*c* (cyt.*c*-CFP), and tetramethylrhodamine methyl ester (TMRM) in order to detect caspase activation, cyt.*c* release from the mitochondria, and mitochondrial depolarization, respectively. By applying two of these probes simultaneously, two events could be monitored in the same cell, and the temporal relationships between caspase activation and mitochondrial changes could be examined at the single-cell level. In addition, we also analyzed the interval from tumor necrosis factor (TNF)-α exposure to cellular shrinkage by analyzing the cell population in order to investigate time course of the whole cell death process.

Materials and Methods

Plasmid construction

A plasmid encoding YRec, YFP-peptide-DsRed, was generated as previously reported (24). The sequence encoding the 11 amino acids at the C-terminus of YFP was eliminated in this construct. The C-terminal-truncated forms of the YFP gene were generated by PCR with primers containing the NheI site or the BspEI site and pEYFP-C1 (Clontech, Palo Alto, CA, USA) as a template, and the restricted fragment was inserted into the NheI/BspEI sites of pEYFP-C1 in order to generate a plasmid carrying truncated YFP. The oligonucleotides encoding the caspase's substrate sequence was inserted into the BspEI – AgeI site of the p(truncated YFP)-C1 vector to generate pYFP-PARP. The substrate sequence was derived from PARP (KRKGDEVDGVDE, 5'-CCGGAAAGAGAAAAGG CGATGAGGTGGATGGAGTGGATGAA-3' and 5'-CCGGTTCATCCACTCCATCCACCTCATCGCCTTT TCTCTTT-3'). DsRed was generated from pDsRed2-C1(Clontech) by PCR, at the AgeI/NotI sites, and the restricted fragment was inserted into the AgeI – NotI sites of pYFP-PARP to generate a plasmid carrying YFP-PARP-DsRed2 (YRec). YRec was cleaved by caspase-3 (23, 24).

Cyt.*c* was cloned from HeLa cells by RT-PCR with a primer pair (5'-TCGCTAGCGCTCCGGAGAATTAAA TATGGGTATG-3' and 5'-CGAGGATCCCTCATTAG TAGCTTTTTTGAG-3'), and the restricted fragment was inserted into the NheI – BamHI sites of the pECFP-N1 vector to generate a plasmid carrying cyt.*c*-CFP. All cloned sequences were verified by sequencing.

Cell culture and transfection

HeLa cells were cultured in DMEM (Sigma-Aldrich, St. Louis, MO, USA) supplemented with 100 units/ml of penicillin G, 100 μg/ml of streptomycin, and 10% fetal calf serum (GIBCO). The plasmid encoding the fluorescent probes was transfected into HeLa cells using Effectene Transfection Reagent (QIAGEN, Hilden, Germany) according to the manufacturer's instructions. After being incubated for 12 – 24 h with the transfection reagent, the cells were washed with PBS and cultivated on dishes suitable for an assay in medium containing 500 μg/ml of G418 for an additional 1 – 3 days until the assay was performed. We found that the cultivation period had no effect on cell death events after TNF-α treatment.

Bioimaging with fluorescence microscopy

Transfected cells were cultured on a cover glass (25-mm diameter, 0.15 – 0.18-mm thickness) for 1 – 3 days. Cells were treated with TNF-α (100 ng/ml, dissolved in PBS) and cycloheximide (10 μg/ml, dissolved in DMSO) and then were incubated under the usual culture conditions for 1 – 2 h prior to the analysis.

Table 1. Measurement conditions for real-time analysis by LSM510

Probe	Excitation (nm)	Beam splitter (nm)	Emission (nm)
Cyt.*c*-CFP	458	515	467.5 – 497.5
YRec	488	545	505 – 530 (donor)[a]
			560 – 615 (acceptor)[a]
TMRM	543	545	560 –[b]

[a]Emitted fluorescence was separated by a 545 dichroic mirror, and the fluorescence of the donor (YFP) and that of the acceptor (DsRed) was obtained via a band-pass emission filter. [b]A long-pass filter (LP560) was used.

Tetramethylrhodamine methyl ester (TMRM; 50 nM, dissolved in DMSO) was added to each sample 20 – 30 min prior to the analysis, when the mitochondrial membrane potential was to be measured (23, 25). Analyses were carried out by confocal laser scanning fluorescent microscopy using a Carl Zeiss LSM510 system (Carl Zeiss, Jena, Germany). During the observations, the media were buffered with 10 mM HEPES buffer (pH 7.4), and the cells were maintained at 35°C – 37°C. DIC images and grayscale images for fluorescence channels were obtained in 0.5- or 1-min intervals. Excitation lights for the cyt.*c*-CFP (458 nm) and YRec (488 nm) were provided by an Ar laser with a 458 or a 488 dichroic mirror, respectively. Excitation lights for the TMRM (543 nm) were provided by a HeNe laser with a 543 dichroic mirror. Images of the probes were obtained separately using a dichroic mirror and band-pass or long-pass emission filters, as indicated in Table 1. Contamination of the fluorescence between channels was negligible under these conditions (data not shown). For analyses involving YRec or TMRM, images were processed and quantified using MetaFluor software as follows: The average pixel intensity of the fluorescence of the entire cell region was determined for each channel. In the case of YRec, the ratio value was calculated as the average pixel value of the fluorescence ratio, (fluorescent intensity for the acceptor channel) /(fluorescent intensity for the donor channel), in the entire cell region. As the cells changed morphologically during the observation, the entire cell region was assessed separately for each image.

Simultaneous measurement of two probes was performed according to the multi-track scanning mode, in which two sets of excitation-detection conditions were used in alternation. For cyt.*c*-CFP and YRec, CFP fluorescence induced by excitation at 458 nm was measured in the first track, and YFP and DsRed fluorescence induced by excitation at 488 nm was measured in the second track. For cyt.*c*-CFP and TMRM, CFP fluorescence induced by excitation at 458 nm was measured in the first track, and TMRM fluorescence induced by excitation at 543 nm was measured in the second track. The scanning time difference between tracks was ca. 3 – 8 s, which was not significant in the temporal analysis.

Analysis of cell survival rate

HeLa cells were cultured in 96-well plastic plates to 80% – 90% confluency and were then treated with TNF-*α*. After the indicated culture durations, the cells were treated with Alamar Blue (Dainippon Pharmaceutical, Osaka) according to the manufacturer's instructions. Cell survival was measured as fluorescence at 590 nm induced by excitation at 540 nm. Fluorescence was measured using FlexStation (Molecular Devices, Sunnyvale, CA, USA).

Results

Simultaneous imaging of cyt.c-CFP and caspase sensor

HeLa cells expressing both cyt.*c*-CFP and YRec were treated with TNF-*α*, and changes in fluorescence were observed. Figure 1A shows DIC images, fluorescent images of CFP, and fluorescence ratio (DsRed/YFP) images of YRec during cell death. Images were obtained every 30 s; therefore, we were able to identify the time points of these events at a resolution period of 30 s. The CFP fluorescence indicated cyt.*c*-CFP localization, and the fluorescence ratio (DsRed/YFP) indicated caspase activation. CFP fluorescence was localized in the mitochondria at 280.5 min, and it was delocalized at 281.0 min, indicating that cyt.*c*-CFP was released during this period. The images shown in Fig. 1A indicate that this cell started to shrink at 286.5 – 287.0 min.

When the caspase was activated in a cell, the YRec was cleaved, which led to a reduction in the FRET from YFP to DsRed. Thus, a reduction in the fluorescence ratio (DsRed/YFP) reflected caspase activation. As shown in Fig. 1B, the fluorescence ratio decreased dramatically at 283.5 min in the cell shown here, thus indicating the initiation of caspase activation at this point in time. The increase in DsRed fluorescence

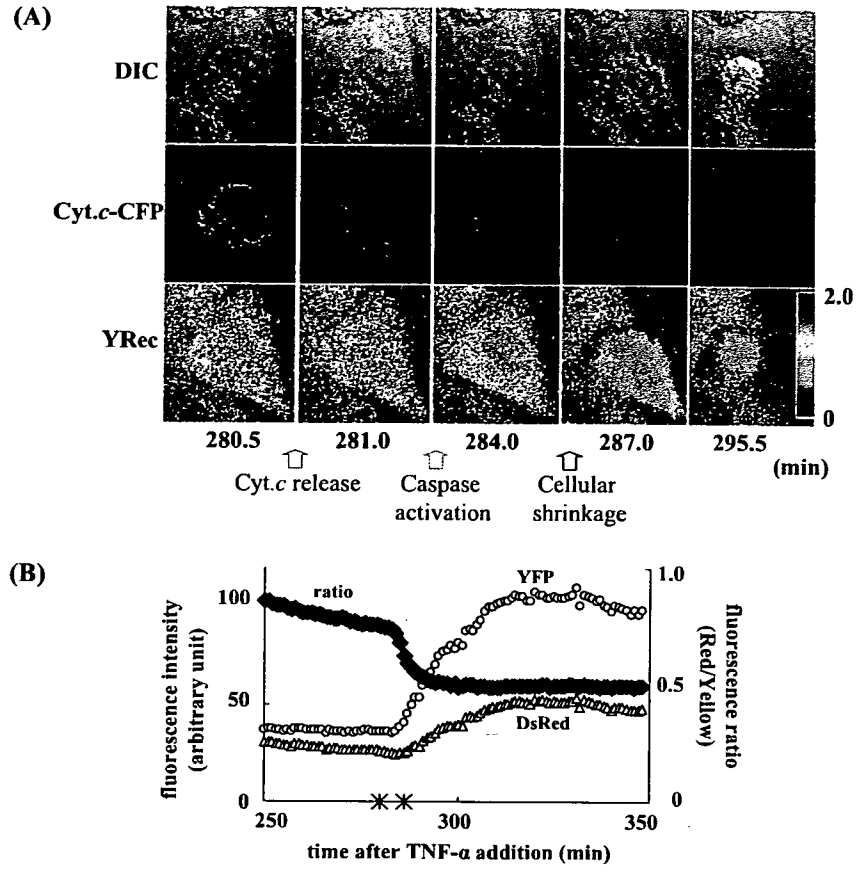

Fig. 1. Cyt.*c*-CFP release and caspase activation were monitored simultaneously in the same cells. A: DIC (upper), images showing the fluorescence of CFP (middle) and the fluorescence ratio of DsRed and YFP (DsRed /YFP, lower) during cell death are shown in pseudocolor. CFP and DsRed/YFP indicate the localization of cyt.*c*-CFP and caspase activation, respectively. B: Changes in YRec fluorescence in the cell shown in panel A were plotted. YFP and DsRed are shown with their fluorescence ratios. The asterisks indicate time points at which cyt.*c*-CFP were released and cell shrinkage was observed. The horizontal axis represents the point in time after the addition of TNF-α.

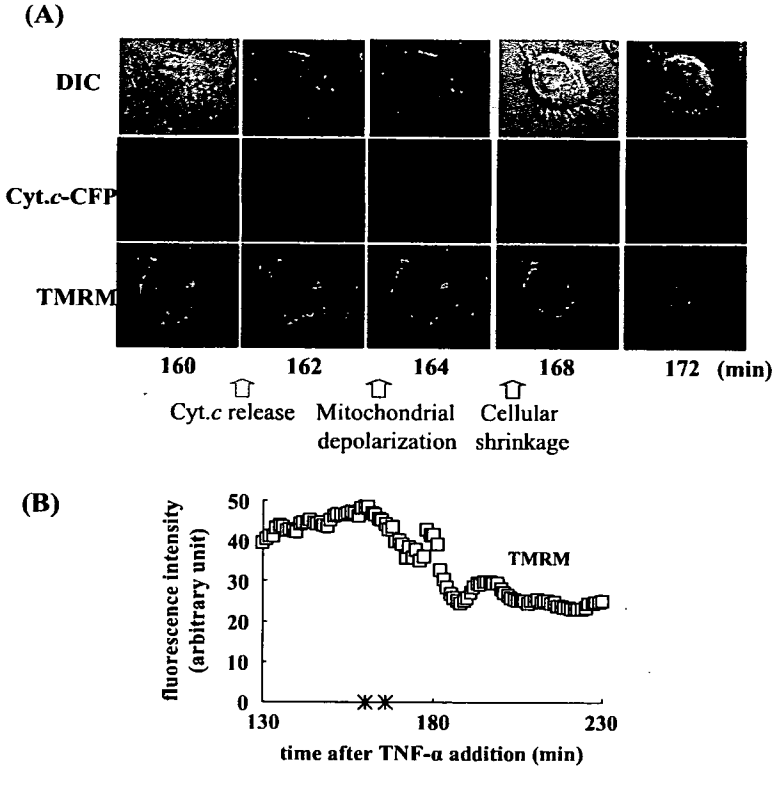

Fig. 2. Cyt.*c*-CFP release and mitochondrial depolarization were monitored simultaneously in the same cell. A: DIC (upper), images showing the fluorescence of CFP (middle) and the fluorescence of TMRM (lower) during cell death are shown in pseudocolor. CFP and TMRM fluorescence indicate the localization of cyt.*c*-CFP and the mitochondrial membrane potential, respectively. B: Changes in TMRM fluorescence of the cells in panel A during cell death were plotted. The asterisks indicate time points at which cyt.*c*-CFP were released and cell shrinkage was observed. The horizontal axis represents the point in time after the addition of TNF-α.

observed after this time point was unexpected, but is thought to have been the result of cellular shrinkage. Because the cell volume was reduced, the DsRed became concentrated, and the fluorescence increased. The reduction in the fluorescence ratio clearly indicated a reduction in FRET, which indicated both the cleavage of YRec as well as caspase activation. The asterisks indicate the time point of cyt.*c*-CFP release and cellular shrinkage, as determined based on the results shown in Fig. 1A. In this cell, cyt.*c*-CFP was released 280.5 min after the addition of TNF-α, and caspase activation was initiated 3 min after cyt.*c*-CFP release; the cell then started to shrink 3 min after caspase activation. Cyt.*c*-CFP release, caspase activation, and cellular shrinkage were observed in this order in all of the dying cells examined.

Simultaneous imaging of cyt.c-CFP and TMRM

HeLa cells expressing cyt.*c*-CFP were treated with TMRM and TNF-α. Delocalization of cyt.*c*-CFP and mitochondrial depolarization were observed with a resolution period of 1 min. All dying cells exhibited cyt.*c*-CFP release, mitochondrial depolarization, and shrinkage of the cell body. Figure 2A shows a typical fluorescent image of a dying cell. In this cell, cyt.*c*-CFP was released at 161 min, and cell shrinkage began at 167 min after the addition of TNF-α. Changes in TMRM fluorescence are plotted in Fig. 2B. TMRM fluorescence started to decrease at 164 min, thus indicating that the mitochondria started to depolarize at this point in time.

In a comparison of the starting points of these three events, it was found that the release of cyt.*c*-CFP always preceded mitochondrial depolarization and cellular shrinkage. Mitochondrial depolarization was observed earlier than cellular shrinkage in this particular cell, but was observed later in other cells. The temporal order of the timing of the initiation of mitochondrial depolarization and cellular shrinkage was not consistent. Mitochondrial depolarization preceded cellular shrinkage in 4 of the 10 cells, and cellular shrinkage preceded mitochondrial depolarization in 6 of the cells observed here.

Temporal relationships between mitochondrial changes, caspase activation, and cellular shrinkage

We observed 10 – 22 cells in each of these experiments, the results of which are shown in Figs. 1 and 2. We then determined the timing of cyt.*c* release, cellular shrinkage, and mitochondrial depolarization, or caspase activation in each cell. To clarify the temporal relationships between these cellular events, relative timing was

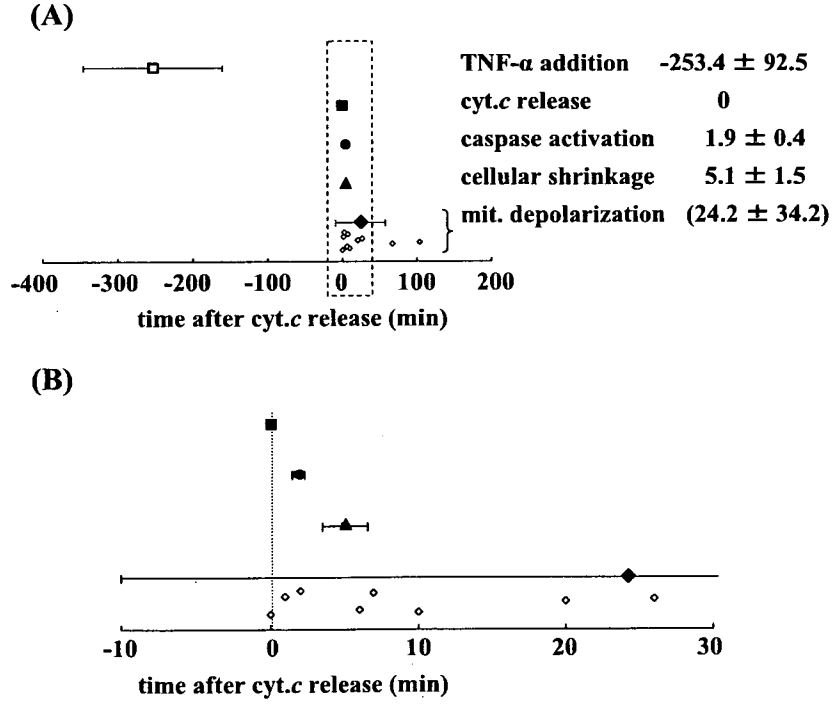

Fig. 3. Temporal relationship between mitochondrial changes and caspase activation. A: Relative timing of TNF-α addition (open square), cyt.*c* release (closed square), caspase activation (closed circle), cellular shrinkage (closed triangle), and mitochondrial depolarization (closed and open diamond) is shown with respect to time after cyt.*c* release. B: Shows a magnification of panel A.

determined as follows: the time point of cyt.*c* release was considered as time 0 in each of the individual cells. We calculated the relative timing of each of the observed events for each cell, and the results are plotted in Fig. 3. TNF-α treatment, cyt.*c* release, caspase activation, and cellular shrinkage are indicated as the mean ± S.D. Since mitochondrial depolarization did not give a normal distribution, all data for mitochondrial depolarization were plotted. Each plot represents the results from a single cell. Figure 3B shows magnification at around time 0.

The relative timing of TNF-α treatment and mitochondrial depolarization was found to deviate substantially, whereas the relative timing of caspase activation and cellular shrinkage gave only a small deviation. A substantial amount of time was required for the initiation of cyt.*c* release, and the duration varied between cells; however, after cyt.*c* release, the subsequent reactions occurred rapidly. After cyt.*c* release, cells are unable to stop or delay the cell death process.

Mitochondrial depolarization occurred before both caspase activation and cellular shrinkage in some of the cells (n = 4), but mitochondrial depolarization occurred after caspase activation and cellular shrinkage in other cells (n = 6). This finding suggests that mitochondrial depolarization is not necessary for either caspase activation or cellular shrinkage. Mitochondrial depolarization has been consistently reported as being associated with cell death, but it is not thought to be a critical step in the induction of apoptotic cell death.

Effects of the duration of TNF-α treatment

At the first step of TNF-α-induced cell death, TNF-α binds with its receptor on the cell surface, and an extracellular signal is transferred into the cell. After this step, Bid transfers the signal to the mitochondria, and then cyt.*c* is released from the mitochondria to the cytosol. Our results shown in Fig. 3 indicate that these processes took about 4 h. In order to analyze the timing of the onset of the earliest steps, we attempted to determine the point in time at which the first step started. To this end, we changed the duration of TNF-α exposure and measured the resulting cell survival rate. Cells were divided to two groups, as shown in Fig. 4A, and the cells were exposed to TNF-α for 0 – 12 h. In group A, the survival rate was measured immediately after TNF-α exposure. In group B, TNF-α was washed off after the indicated exposure time, and the cells were cultured in fresh medium without TNF-α for an additional 6 – 11 h, and the survival rate was then measured. If the cell death process proceeded after the removal of TNF-α, the survival rate would be expected to be reduced due to the additional culture period after the removal of TNF-α. In other words, more cells would be expected to have died in group B than in group A with the same amount of TNF-α exposure time.

The results showed that the survival rate decreased with increasing TNF-α exposure time (Fig. 4B). However, the survival rate did not decrease after TNF-α removal. This result suggests that the dead cells in group B had died during the period of TNF-α exposure, and that those cells that had survived during TNF-α exposure did not die after the removal of TNF-α. Thus, the cell death process is likely to proceed only when the cells were exposed to TNF-α. The survival rate in group B increased when cells were exposed TNF-α for 6 h. The biological meaning of this increase was unknown; however, this result did not disturb our conclusion.

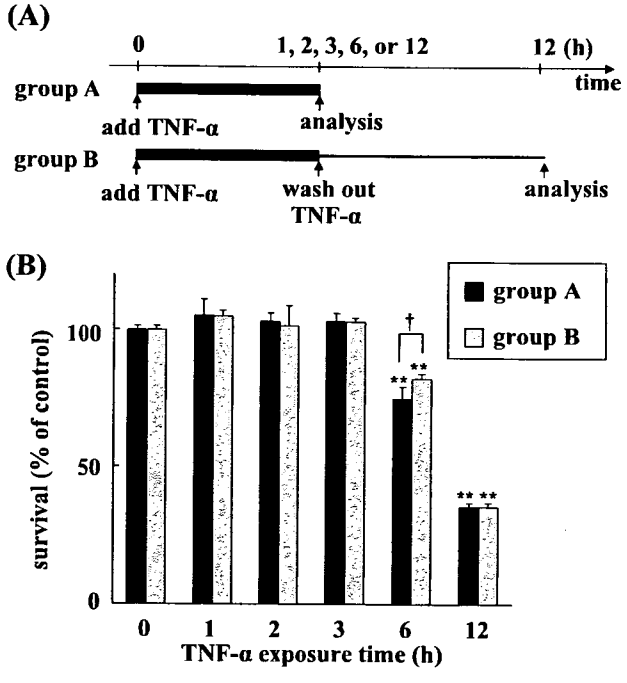

Fig. 4. Cell survival rate after TNF-α exposure. Panel A: Experimental design of the TNF-α exposure analysis. Thick lines represent the incubation in the presence of TNF-α, and thin line represents the incubation in the absence of TNF-α. In group A, cells were exposed to TNF-α for the indicated amount of time, and the cell survival rate was measured immediately. In group B, cells were exposed in the same manner as that used for group A. Then, the TNF-α was washed out, and the cells were cultured in fresh media for 6 – 11 h. Then, the cell survival rate was measured. The total duration of the culture period after the onset of TNF-α exposure was 12 h in group B. Panel B: The cells in groups A and B were exposed to TNF-α for 1, 2, 3, 6, or 12 h, and the cell survival rates were determined. Each bar represents a mean ± S.D. (n = 6). $^{**}P<0.01$ *vs* time 0, according to Dunnett's test. $^{\dagger}P<0.05$ between groups A and B, according to Student's *t*-test.

Discussion

This is the first report to reveal the precise temporal relationships between four reactions (mitochondrial depolarization, cyt.*c* release, caspase activation, and cellular shrinkage) in TNF-α-induced cell death. Because the onset of these reactions varied among individual cells, real-time single-cell imaging is the only currently available method to reveal temporal relationships between these reactions. We described our three-color real-time imaging technique in this report. Rehm et al. has reported the simultaneous real-time imaging of caspase activation and Smac release by using CFP/YFP-FRET sensor and YFP-tagged protein (26). They used the same color, YFP, for the observation of both reactions. It is possible to identify two reactions as they discussed, but it may be difficult to identify small changes occurring in the cell by their method. Previously, we revealed that DsRed was useful for FRET analysis of caspase activation (24). In this report, we observed caspase activation and cyt.*c* release with YFP/DsRed-FRET sensor and CFP-tagged protein. By using fluorescent probes in different colors, each reaction could be easily and precisely identified in a single cell.

We observed cell death at the single-cell level with a resolution period of 0.5 – 1 min, and we revealed that the relative timing between cyt.*c* release, caspase activation, and cellular shrinkage remained constant in all of the dying cells observed; however, the timing of mitochondrial depolarization showed a large deviation (Fig. 3). After cyt.*c* release, apoptosome formation, caspase-9 activation, caspase-3 activation, and the cleavage of various substrates that lead to apoptotic cell death are initiated. Our results revealed that this series of reactions takes place within 10 min and that the time course of this process was identical among all of the dying HeLa cells.

Mitochondrial depolarization was observed in all dying cells, but we considered that mitochondrial depolarization was not the cause of cyt.*c* release, caspase activation, and cellular shrinkage. Mitochondrial depolarization was found to occur at any time after cyt.*c* release. Mitochondrial depolarization was observed after caspase activation and cellular shrinkage in 60% of the observed cells. These results exclude the possibility that mitochondrial depolarization is a cause of cyt.*c* release, caspase activation, and/or cellular shrinkage. This is consistent with previous findings that cell death occurred without mitochondrial depolarization. Li et al. have shown that caspases are activated independently of mitochondrial depolarization in TNF-α-induced cell death (27). Krohn et al. have shown that cyt.*c* release and caspase activation occurred in the absence of mitochondrial depolarization in cell death of hippocampal neurons (28). Several studies suggested that mitochondrial depolarization is a critical step for cell death (29), but our results support the idea that mitochondrial depolarization is not crucial to the cell death process.

Cyt.*c* release may be a key step in two independent series of events, that is, the cell death process and mitochondrial depolarization. We speculate that cells might try to maintain cellular homeostasis by keeping membrane potential after cyt.*c* release. While maintaining the membrane potential, the released cyt.*c* immediately initiated the cell death process in the cytosol, and thus caspase activation and cellular shrinkage always took place within a short period of time. The timing of mitochondrial depolarization did not appear to be relevant to this process.

A number of imaging analyses have demonstrated that each cell death event is a rapid process. Initiator- and effector-caspase activation both proceed rapidly (23, 24, 30 – 32). Cyt.*c* is also released rapidly in a single step (33 – 35). Likewise, Smac/DIABLO is released rapidly, although the duration of Smac/DIABLO release is greater than that of cyt.*c* (26). Several multi-event imaging studies have suggested that cell death events occur almost simultaneously. Initiator caspase activation/effector caspase activation, effector caspase activation/mitochondrial depolarization, cyt.*c*/smac, and effector caspase activation/smac release had been analyzed simultaneously at the single-cell level and were found to occur almost simultaneously (24, 26). These findings, taken together with our present results, suggest that the cell death cascade proceeds rapidly after mitochondrial changes take place.

Once cyt.*c* was released, the following reactions proceed in a rapid manner. However, it did take 253.4 ± 92.5 min from TNF-α treatment to cyt.*c* release, and this duration varied from cell to cell (Figs. 3 and 4). We observed some cells that had died within 1 h in imaging analysis, indicating that cells have the ability to induce cell death within 1 h, and suggesting that certain factors may delay signal transduction and the timing of cell death. The results shown in Fig. 4 indicate that these factors were active only when the cells were exposed to TNF-α. We considered two possible explanations for these findings. 1: Each TNF-α molecule changed the cell slightly, and the changes induced by one molecule were not sufficient to induce the cell death cascade on their own. However, many TNF-α molecules attacked the cell, and intracellular changes thus accumulated. When the accumulated changes exceeded the threshold level, the cell death cascade would be expected to have

proceeded rapidly. 2: TNF-α could induce intracellular changes by chance. According to this explanation, TNF-α molecules would bind with the TNF receptor, but only some of them would be able to induce intracellular change. If some TNF-α molecules successfully induce intracellular changes, then the cell death cascade would proceed rapidly. The more TNF-α molecules that are present around the cell, and/or the longer these TNF-α molecules attack the cell, the higher the probability of a successful attack, and it can be expected that more cells will die. According to both of these models, the cell death process would not proceed in the absence of TNF-α exposure; therefore, those cells that survived during TNF-α exposure would not be expected to die after the removal of TNF-α.

One of the Bcl-2 family proteins, Bid, was cleaved to tBid due to the cell death signal, and the tBid transferred the signal from the cytosol to the mitochondria (36). Exogenous treatment with tBid is known to induce cell death immediately (37), and thus reactions that delay signal transduction may occur at an earlier step than either Bid cleavage or mitochondrial changes.

As cell death reactions often occur in a rapid manner and because the timing of the onset of intracellular reactions varies among cells, precise temporal relationships between cellular events during cell death should be further analyzed at the single-cell level with high temporal resolution. Single-cell imaging analyses of early stages (e.g., receptor oligomerization and the recruitment of adaptor proteins) will help to elucidate the mechanism of the entire cell death process.

Acknowledgments

This study was supported in part by a Grant-in-Aid for Research on Health Sciences focusing on Drug Innovation from the Japan Health Science Foundation; a Grant-in-Aid for Research on Advanced Medical Technology from the Ministry of Health, Labour, and Welfare; and a grant (MF-16) from the Organization for Pharmaceutical Safety and Research.

References

1 Thornberry NA, Lazebnik Y. Caspases: enemies within. Science. 1998;281:1312–1316.
2 Stennicke HR, Salvesen GS. Properties of caspases. Biochim Biophys Acta. 1998;1387:17–31.
3 Boldin MP, Goncharov TM, Goltsev YV, Wallach D. Involvement of MACH, a novel MORT1/FADD-interacting protease, in Fas/APO-1- and TNF receptor-induced cell death. Cell. 1996; 85:803–815.
4 Muzio M, Chinnaiyan AM, Kischkell FC, O'Rourke K, Shevchenko A, Ni J, et al. FLICE, a novel FADD-homologous ICE/CED-3-like protease, is recruited to the CD95 (Fas/APO-1) death-inducing signal complex. Cell. 1996;85:817–827.
5 Medema JP, Scaffidi C, Kischkel FC, Shevchenko A, Mann M, Krammer PH, et al. FLICE is activated by association with the CD95 death-inducing signaling complex (DISC). EMBO J. 1997;16:2794–2804.
6 Martin DA, Siegel RM, Zheng L, Lenardo MJ. Membrane oligomerization and cleavage activates the caspase-8 (FLICE /MACHalpha1) death signal. J Biol Chem. 1998;273:4345–4349.
7 Srinivasula SM, Ahmad M, Fernandes-Alnemri T, Litwack G, Alnemri ES. Molecular ordering of the Fas-apoptotic pathway: The Fas/APO-1 protease Mch5 is a CrmA-inhibitable protease that activates multiple Ced-3/ICE-like cysteine proteases. Proc Natl Acad Sci U S A. 1996;93:14486–14491.
8 Orth K, O'Rourke K, Salvesen GS, Dixit VM. Molecular ordering of apoptotic mammalian CED-3/ICE-like proteases. J Biol Chem. 1996;271:20977–20980.
9 Tewari M, Quan LT, O'Rourke K, Desnoyers S, Zeng Z, Beidler DR, et al. Yama/CPP32 beta, a mammalian homolog of CED-3, is a CrmA-inhibitable protease that cleaves the death substrate poly(ADP-ribose) polymerase. Cell. 1995;81:801–809.
10 Green DR, Reed JC. Mitochondria and apoptosis. Science. 1998;281:1309–1312.
11 Martinou JC, Green DR. Breaking the mitochondrial barrier. Nat Rev Mol Cell Biol. 2001;2:63–67.
12 Saleh A, Srinivasula SM, Acharya S, Fishel R, Alnemri ES. Cytochrome c and dATP-mediated oligomerization of Apaf-1 is a prerequisite for procaspase-9 activation. J Biol Chem. 1999;274:17941–17945.
13 Shiozaki EN, Chai J, Shi Y. Oligomerization and activation of caspase-9, induced by Apaf-1 CARD. Proc Natl Acad Sci U S A. 2002;99:4197–4202.
14 Tyas L, Brophy VA, Pope A, Rivett AJ, Tavare JM. Rapid caspase-3 activation during apoptosis revealed using fluorescence-resonance energy transfer. EMBO reports. 2000;1:266–270.
15 Rehm M, Dussmann H, Janicke RU, Tavare JM, Kogel D, Prehn JHM. Single-cell fluorescence resonance energy transfer analysis demonstrates that caspase activation during apoptosis is a rapid process: role of caspase-3. J Biol Chem. 2002;277: 24506–24514.
16 Luo KQ, Yu VC, Pu Y, Chang DC. Application of the fluorescence resonance energy transfer method for studying the dynamics of caspase-3 activation during UV-induced apoptosis in living HeLa cells. Biochem Biophys Res Commun. 2001;283:1054–1060.
17 Morgan MJ, Thorburn A. Measurement of caspase activity in individual cells reveals differences in the kinetics of caspase activation between cells. Cell Death Differ. 2001;8:38–43.
18 Tsien RY, Miyawaki A. Seeing the machinery of live cells. Science. 1998;280:1954–1955.
19 Miyawaki A, Sawano A, Kogure T. Lighting up cells: labeling proteins with fluorophores. Nat Cell Biol. 2003;S1–S7.
20 Tsien RY, The green fluorescent protein. Annu Rev Biochem. 1998;67:509–544.
21 Erickson MG, Moon DL, Yue DT. DsRed as a potential FRET partner with CFP and GFP. Biophys J. 2003;85:599–611.
22 Karasawa S, Araki T, Nagai T, Mizuno H, Miyawaki A. Cyan-emitting and orange-emitting fluorescent proteins as a donor

/acceptor pair for fluorescence resonance energy transfer. Biochem J. 2004;381:307–312.
23 Kawai H, Suzuki T, Kobayashi T, Mizuguchi H, Hayakawa T, Kawanishi T. Simultaneous imaging of initiator / effector caspase activity and mitochondrial membrane potential during cell death in living HeLa cells. Biochim Biophys Acta. 2004;1693:101–110.
24 Kawai H, Suzuki T, Kobayashi T, Sakurai H, Ohata H, Honda K, et al. Simultaneous real-time detection of initiator- and effector-caspase activation by double fluorescence resonance energy transfer analysis. J Pharmacol Sci. 2005;97:361–368.
25 Scaduto RC Jr, Grotyohann LW. Measurement of mitochondrial membrane potential using fluorescent rhodamine derivatives. Biophys J. 1999;76:469–477.
26 Rehm M, Dussmann H, Prehn JHM. Real-time single cell analysis of Smac/DIABLO release during apoptosis. J Cell Biol. 2003;162:1031–1043.
27 Li X, Du L, Darzynkiewicz Z. During apoptosis of HL-60 and U-937 cells caspases are activated independently of dissipation of mitochondrial electrochemical potential. Exp Cell Res. 2000;257:290–297.
28 Krohn AJ, Wahlbrink T, Prehn JHM. Mitochondrial depolarization is not required for neuronal apoptosis. J Neurosci. 1999;19:7394–7404.
29 Heiskanen KM, Bhat MB, Wang H-W, Ma J, Nieminen A-L. Mitochondrial depolarization accompanies cytochrome c release during apoptosis in PC6 cells. J Biol Chem. 1999;274:5654–5658.
30 Ohnuki R, Nagasaki A, Kawasaki H, Baba T, Uyeda TQP, Taira K. Confirmation by FRET in individual living cells of the absence of significant amyloid β-mediated caspase 8 activation. Proc Natl Acad Sci U S A. 2002;99:14716–14721.
31 Takemoto K, Nagai T, Miyawaki A, Miura M. Spatio-temporal activation of caspase revealed by indicator that is insensitive to environmental effects. J Cell Biol. 2003;160:235–243.
32 Luo KQ, Yu VC, Pu Y, Chang DC. Measuring dynamics of caspase-8 activation in a single living HeLa cell during TNFalpha-induced apoptosis. Biochem Biophys Res Commun. 2003;304:217–222.
33 Lim MLR, Lum M-G, Hansen TM, Roucou X, Nagley P. On the release of cytochrome c from mitochondria during cell death signaling. J Biomed Sci. 2002;9:488–506.
34 Goldstein JC, Waterhouse NJ, Juin P, Evan GI, Green DR. The coordinate release of cytochrome c during apoptosis is rapid, complete and kinetically invariant. Nat Cell Biol. 2000;2:156–162.
35 Goldstein JC, Munoz-Pinedo C, Ricci J-E, Adams SR, Kelekar A, Schuler M, et al. Cytochrome c is released in a single step during apoptosis. Cell Death Differ. 2005;12:453–462.
36 Luo X, Budihardjo I, Zou H, Slaughter C, Wang X. Bid, a Bcl-2 interacting protein, mediates cytochrome c release from mitochondria in response to activation of cell surface death receptors. Cell. 1998;94:481–490.
37 Madesh M, Antonsson B, Srinivasula SM, Alnemri ES, Hajnóczky G. Rapid kinetics of tbid-induced cytochrome *c* and Smac/DIABLO release and mitochondrial depolarization. J Biol Chem. 2002;277:5651–5659.

J Pharmacol Sci 103, 241 – 246 (2007)

Journal of Pharmacological Sciences

Full Paper

Involvement of the Na^+/Ca^{2+} Exchanger in Ouabain-Induced Inotropy and Arrhythmogenesis in Guinea-Pig Myocardium as Revealed by SEA0400

Hikaru Tanaka[1,*], Hideaki Shimada[1], Iyuki Namekata[1], Toru Kawanishi[2], Naoko Iida-Tanaka[1,3], and Koki Shigenobu[1]

[1]*Department of Pharmacology, Toho University Faculty of Pharmaceutical Sciences, Funabashi, Chiba 274-8510, Japan*
[2]*Division of Biological Chemistry and Biologicals, National Institute of Health Sciences, Tokyo 158-8501, Japan*
[3]*Department of Food Science, Otsuma Woman's University, Chiyoda-ku, Tokyo 102-8357, Japan*

Received August 10, 2006; Accepted December 19, 2006

Abstract. Involvement of the Na^+/Ca^{2+} exchanger in ouabain-induced inotropy and arrhythmogenesis was examined with a specific inhibitor, SEA0400. In right ventricular papillary muscle isolated from guinea-pig ventricle, 1 μM SEA0400, which specifically inhibits the Na^+/Ca^{2+} exchanger by 80%, reduced the ouabain (1 μM)-induced positive inotropy by 40%, but had no effect on the inotropy induced by 100 μM isobutyl methylxantine. SEA0400 significantly inhibited the contracture induced by low Na^+ solution. In HEK293 cells expressing the Na^+/Ca^{2+} exchanger, 1 μM ouabain induced an increase in intracellular Ca^{2+}, which was inhibited by SEA0400. The arrhythmic contractions induced by 3 μM ouabain were significantly reduced by SEA0400. These results provide pharmacological evidence that the Na^+/Ca^{2+} exchanger is involved in ouabain-induced inotropy and arrhythmogenesis.

Keywords: ouabain, Na^+/Ca^{2+} exchanger, SEA0400, inotropy, arrhythmia

Introduction

The Na^+/Ca^{2+} exchanger (NCX) is involved in the physiological and pathophysiological regulation of Ca^{2+} concentration in the myocardium. It is considered to function both in the forward (Ca^{2+} extrusion) and reverse (Ca^{2+} influx) modes. The major role of myocardial NCX is to extrude Ca^{2+} from the cell through the forward mode and produce relaxation. Contribution of reverse mode NCX to Ca^{2+} entry during the early phase of normal myocardial contraction has also been postulated. The mode of NCX action possibly changes during the contractile cycle and the balance may vary with factors such as the animal species, developmental stage and the condition of the myocardium (1, 2). NCX activity is closely related to intracellular Ca^{2+} handling and is involved in normal and abnormal myocardial pacemaking (3).

*Corresponding author. htanaka@phar.toho-u.ac.jp
Published online in J-STAGE
doi: 10.1254/jphs.FP0060911

NCX has also been considered to be involved in cardiac glycoside-induced positive inotropy (4). Cardiac glycosides, which inhibit the sodium-potassium pump, would increase intracellular Na^+ concentration, which in turn shifts the mode of NCX towards the reverse mode, and produce positive inotropy through an increase in intracellular Ca^{2+} concentration. Extensive evidence has been presented for this view including studies with fetal myocardial tubes from NCX knockout mouse (5). However, pharmacological assessment of the role of NCX in cardiac glycoside-induced inotropy and arrhythmogenesis has been limited because of the lack of an NCX inhibitor with sufficient specificity.

SEA0400 {2-[4-[(2,5-difluorophenyl)methoxy]phenoxy]-5-ethoxyaniline} is a potent and selective inhibitor of NCX in cultured rat neurons, astrocytes, microglia, and myocytes and dog sarcolemmal vesicles with negligible affinities towards other transporters, ion channels, and receptors (6 – 9). We have previously examined the effects of SEA0400 on the myocardial NCX current using voltage clamped guinea-pig ventricular myocytes (7) and found that SEA0400 concentra-

tion-dependently inhibits the NCX current with IC_{50} values of 40 and 32 nM for the forward and reverse modes, respectively. This was confirmed with NCX1 expressed in HEK93 cells (10). SEA0400 (1 μM), which inhibited NCX current by more than 80%, had no effect on the Na^+ current, L-type Ca^{2+} current, delayed rectifier K^+ current, and inwardly rectifying K^+ current (7) and the Ca^{2+} sensitivity of contractile proteins (11). KB-R7943, which has been used as an inhibitor of NCX, was revealed to have virtually no selectivity for these ion channels and transporters (7). Thus, SEA0400 can become the first specific pharmacological tool to study the role of NCX and was shown to be useful in studies on myocardial excitation-contraction mechanisms, regulation by autonomic transmitters, and ischemia-reperfusion injury (6, 11 – 17).

Concerning the action of cardiac glycosides, inhibition by SEA0400 of digitalis-induced arrhythmias in canine models was reported (18), but the mechanisms of cardiac glycoside-induced inotropy and arrhythmogenesis has not been examined in the isolated working myocardium with this selective inhibitor. The present study was performed to obtain pharmacological evidence for the involvement of NCX in cardiac glycoside-induced inotropy and arrhythmogenesis.

Materials and Methods

Measurement of contractile force and contracture in papillary muscle preparations

Isolated papillary muscle preparations were made, and contractile force was measured with standard techniques as described (19). Contracture induced by a low sodium solution was used as an index of reverse-mode NCX activity as described earlier (20) with a slightly modified protocol. The initial extracellular solution was of the following composition and gassed with 95% O_2 – 5% CO_2: 113.1 mM NaCl, 4.6 mM KCl, 2.45 mM $CaCl_2$, 1.2 mM $MgCl_2$, 21.9 mM $NaHCO_3$, and 10 mM glucose (pH 7.4). After the contractile force reached the steady state, stimulation was ceased. The preparation was incubated for 30 min with or without 1 μM SEA0400, and thereafter the solution was changed to a low-sodium solution. The low-sodium solution was prepared with the equimolar substitution of tetramethyl-ammonium chloride for NaCl in a modified Krebs solution, so that the final Na^+ concentration was 21.9 mM. This solution also contained 10 μM monensin, 20 mM caffeine, and 4.9 mM $CaCl_2$. The amplitude of low-sodium contracture was expressed as the percentage of steady-state developed tension. SEA0400 (1 μM) was applied from 30 min before the low-sodium perfusion and kept in the low-sodium solution continuously.

Preparation of HEK293 cells expressing NCX and measurement of cytoplasmic Ca^{2+} concentration

HEK293 cells stablly expressing bovine NCX1 were obtained in our previous study (10). Cytoplasmic Ca^{2+} was monitored with the fluorescent probe fura 2. The cells were loaded with 5 μM fura 2/AM for 30 min at 37°C. They were excited at 340 and 380 nm, and emission (>500 nm) was separated with a dichroic mirror. Data acquisition and analysis were performed with the aquacosmos system (Hamamatsu Photonics, Hamamatsu). Calibration was performed *in situ* as in our previous study (17).

Drugs and chemicals

SEA0400 was provided by Taisho Pharmaceutical Company, Ltd. (Saitama). The drug was dissolved in dimethyl sulfoxide (final concentration of 0.01%). Fura 2 was obtained from Dojin (Kumamoto). All other chemicals were of the highest commercially available quality.

Data and statistics

Statistical significance between means was evaluated by Student's *t*-test or by the χ^2-test, and a P value less than 0.05 was considered significant.

Results

Effect of SEA0400 on contracture induced by low-sodium solution

The inhibitory activity of SEA0400 on reverse mode NCX was confirmed in myocardial tissue preparations (Fig. 1). Treatment of ventricular tissue preparations with a low Na^+ extracellular solution resulted in muscle contracture. SEA0400 (1 μM) significantly decreased the contracture; the magnitude of the contracture in the absence and presence of SEA0400 at 30 min was 134.7 ± 34.2% and 43.4 ± 18.4% (n = 10), respectively, of the initial contractile force.

Effect of SEA0400 on ouabain-induced inotropy

Effect of SEA0400 on ouabain-induced inotropy was examined in papillary muscles isolated from guinea-pig right ventricle (Fig. 2). SEA0400 showed no significant inotropic effects; the contractile force after the application of 1 μM SEA0400 was 105.3 ± 10.0% (n = 6) of that before application. Ouabain (1 μM) induced a gradual increase in contractile force; the contractile force at 30 min after addition of ouabain was 473.5 ± 44.7% (n = 6) of that before addition. SEA0400 (1 μM) significantly reduced the ouabain-induced

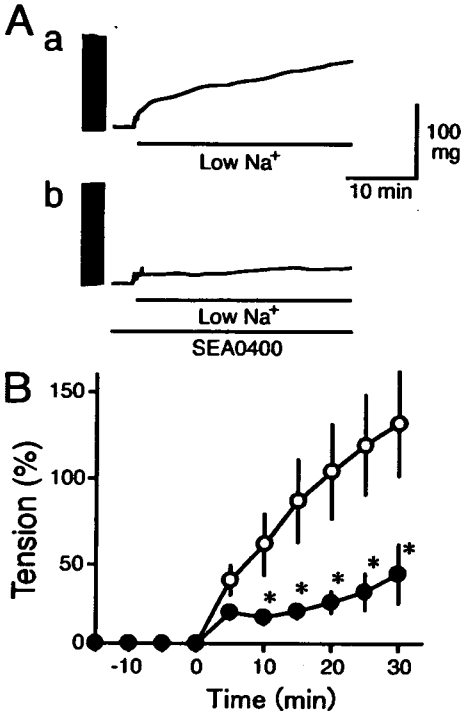

Fig. 1. Effect of SEA0400 on low Na^+-induced contracture in papillary muscles. A: Typical records of contracture induced by low Na^+ solution in the absence (a) and presence (b) of 1 μM SEA0400. B: Summarized results for the contracture. Increase in basal tension was expressed as a percentage of the stimulation-evoked contractile force in the same preparation. Each point with vertical bars represents the mean ± S.E.M. of 10 experiments. Asterisks indicate significant difference ($P<0.05$) from the corresponding values in the absence (open circles) of SEA0400.

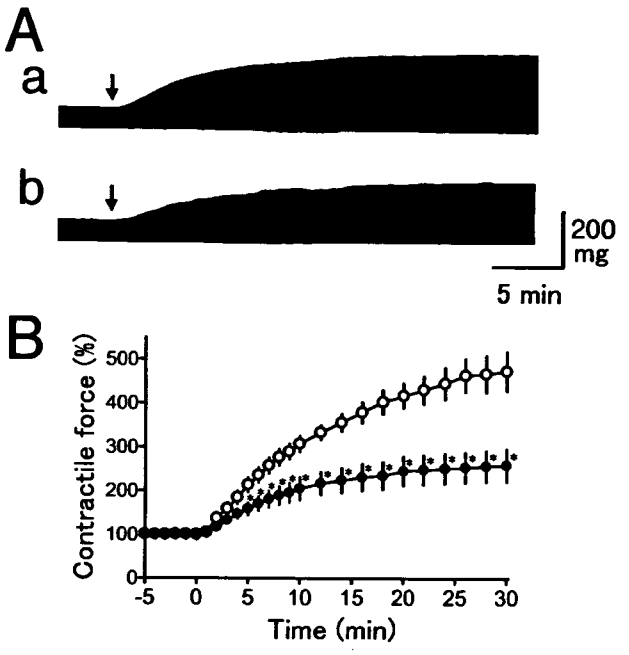

Fig. 2. Effects of SEA0400 on ouabain-induced inotropy. A: Typical records showing the effects of 1 μM ouabain in the absence (a) and presence (b) of 1 μM SEA0400. Arrows indicate the addition of 1 μM ouabain. B: Summarized results in the absence (open circles) and presence (closed circles) of SEA0400. Contractile force after the addition of 1 μM ouabain was expressed as a percentage of the contractile force before the addition. Each point with vertical bar represents the mean ± S.E.M. of 6 experiments. Asterisks indicate significant difference ($P<0.05$) from the corresponding values in the absence of SEA0400.

positive inotropy; in the presence of 0.3, 1, and 10 μM SEA0400, the contractile force at 30 min after addition of ouabain was 394.1 ± 32.9% (n = 6), 259.3 ± 37.1% (n = 6), and 279.8 ± 32% (n = 7) of that before addition, respectively.

Effect of SEA0400 on IBMX-induced inotropy

Effect of SEA0400 on IBMX-induced inotropy was examined in the papillary muscles (Fig. 3). IBMX (100 μM) induced a rapid increase in contractile force; the contractile force at 5 min after addition of ouabain was 281.7 ± 19.4% (n = 6) of that before addition. SEA0400 (1 μM) did not affect the IBMX-induced positive inotropy; in the presence of SEA0400, the contractile force at 30 min after addition of IBMX was 280.7 ± 19.4% (n = 6) of that before addition.

Dependence of ouabain effects on NCX

Dependence of ouabain effects on NCX was examined with HEK293 cells (Fig. 4). Treatment of HEK293cells expressing the NCX1 protein with low Na^+ solution resulted in an increase in cytoplasmic Ca^{2+} concentration that reflects reverse mode NCX activity. In such cells, ouabain induced a gradual increase in cytoplasmic Ca^{2+} concentration. The cytoplasmic Ca^{2+} concentration before and 20 min after the addition of 10 μM ouabain was 46.4 ± 4.5 and 621.5 ± 57.3 nM (n = 17), respectively. This ouabain-induced increase in cytoplasmic Ca^{2+} concentration was completely inhibited by SEA0400. In the presence of 1 μM SEA0400, the cytoplasmic Ca^{2+} concentration before and 20 min after the addition of 10 μM ouabain was 58.8 ± 8.0 and 37.9 ± 7.8 nM (n = 17), In wild type HEK293 cells, the lack of functional NCX activity was confirmed by lack of increase in cytoplasmic Ca^{2+} concentration by low Na^+ solution. Ouabain induced no significant increase in cytoplasmic Ca^{2+} concentration in wild type HEK293 cells, indicating the dependence of ouabain action on NCX function. In wild type HEK293 cells, the cytoplasmic Ca^{2+} concentration before and 20 min after the addition of 10 μM ouabain was 45.2 ± 8.4 and 54.7 ± 8.6 nM (n = 24) (not shown in the figure).

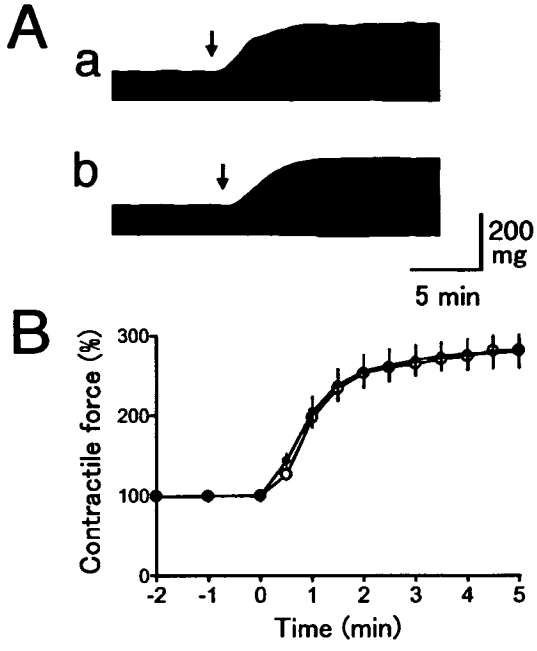

Fig. 3. Effects of SEA0400 on IBMX-induced inotropy. A: Typical records showing the effects of 100 μM IBMX in the absence (a) and presence (b) of 1 μM SEA0400. Arrows indicate the addition of 100 μM IBMX. B: Summarized results in the absence (open circles) and presence (closed circles) of SEA0400. Contractile force after the addition of 100 μM IBMX was expressed as a percentage of the contractile force before the addition. Each point with vertical bar represents the mean ± S.E.M. of 6 experiments.

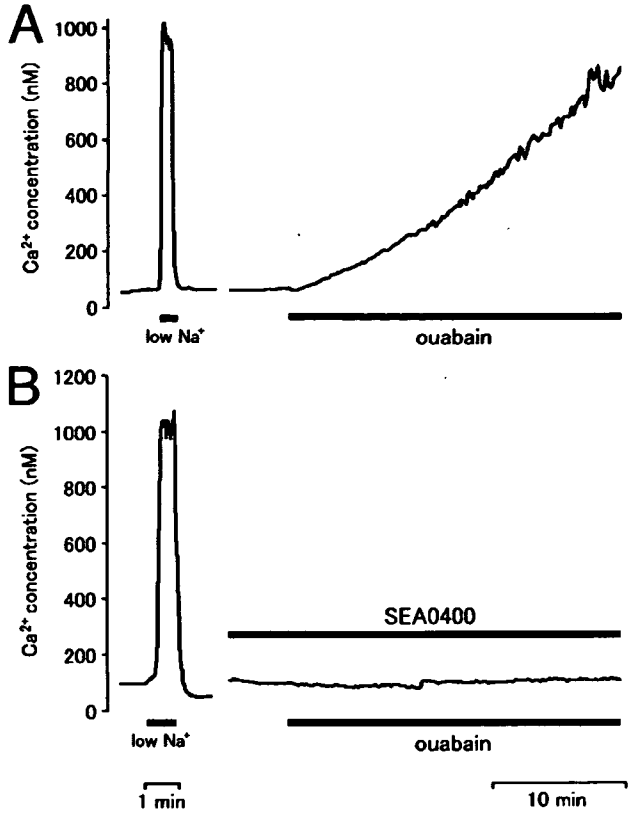

Fig. 4. Effect of ouabain on intracellular Ca^{2+} in HEK293 cells expressing NCX loaded with fura-2. Typical records of changes in intracellular Ca^{2+} concentration in response to 10 μM ouabain in the absence (A) and presence (B) of 1 μM SEA0400. Expression of functional NCX in the cells observed was confirmed by the increase in intracellular Ca^{2+} in response to low Na^+ solution.

Effect of SEA0400 on ouabain-induced arrhythmia

Effect of SEA0400 on ouabain-induced arrhythmia was examined in papillary muscles (Fig. 5). Application of 3 μM ouabain to papillary muscles induced positive inotropy; the contractile force at 10 min after the addition of ouabain increased to 272.7 ± 24.8% (n = 26) of that before the addition. This was followed by the appearance of arrhythmic contraction during the period between 10 and 60 min after ouabain application in 19 out of 26 preparations. The arrhythmic contractions were larger than the stimulation-evoked periodic contractions. After 20 min, oscillatory aftercontractions with decremental amplitude were observed instead of the large arrhythmic contractions. In addition to these changes, 3 μM ouabain induced contracture; the basal tension at 30 min after the addition of ouabain was 305.0 ± 67.1% (n = 26) of the contractile force in the absence of ouabain.

In the presence of 1 μM SEA0400, the ouabain-induced positive inotropy was smaller than that in the absence of SEA0400; contractile force at 10 min was 239 ± 22.7% (n = 26) of that before ouabain addition. The arrhythmic contraction during the period between 10 and 60 min was observed in 12 out of 26 preparations

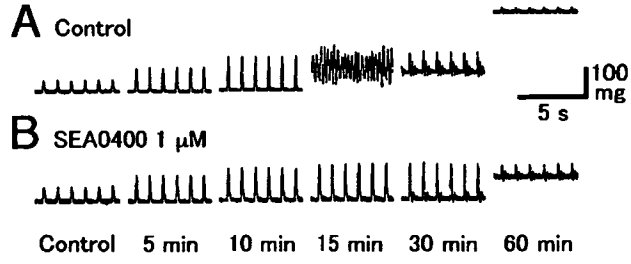

Fig. 5. Effect of SEA0400 on ouabain-induced arrhythmogenesis. Typical records of the contractile response of papillary muscles to 3 μM ouabain in the absence (A) and presence (B) of 1 μM SEA0400. Note that SEA0400 inhibited arrhythmic contractions and reduced the elevation of basal tension.

in the presence of SEA0400; the incidence was significantly smaller than in the absence of SEA0400. The oscillatory aftercontractions observed after 20 min were not inhibited by SEA0400 but the elevation of basal tension was significantly reduced by SEA0400. The

basal tension at 30 min after the addition of ouabain in the presence of SEA0400 was 184.8 ± 55.5% (n = 26) of the contractile force in the absence of ouabain.

Discussion

In isolated guinea-pig papillary muscles, SEA0400 reduced the contracture induced by a low-sodium solution (Fig. 1) indicating that it could inhibit Ca^{2+} influx through NCX not only in cardiomyocytes (7), but also in myocardial tissue. SEA0400 also attenuated the elevation of basal tension during late experimental ischemia (16), which is considered to reflect the inhibition of Ca^{2+} influx through the reverse mode NCX. SEA0400 produced concentration-dependent positive inotropy in mouse ventricular myocardium (11). When the effect of SEA0400 on NCX was examined in voltage clamped guinea-pig ventricular myocytes, SEA0400 inhibited both forward and reverse modes with the same potency (7). SEA0400 increased the contractile force of guinea-pig papillary preparations, suggesting that SEA0400 inhibits Ca^{2+} extrusion through the forward mode NCX in tissue preparations. However, the effect of NCX inhibition by SEA0400 on the forward and reverse modes may not be the same in tissue preparations where the membrane potential and ionic conditions change during the action potential cycle.

Concerning species difference in the positive inotropic effect, SEA0400 (1 μM) increased the contractile force of papillary muscle preparations by only 5% (present study) or less (16) in the guinea pig, but by 25% in the mouse (11). In the guinea-pig ventricle, the membrane potential is more negative than the equilibrium potential of NCX only during the resting period when the intracellular Ca^{2+} is low. In contrast, the mouse has a short duration and higher intracellular Na^+ concentration, which favors Ca^{2+} extrusion through the forward mode NCX during early diastole when the intracellular Ca^{2+} is still elevated (1). Thus, NCX inhibition would result in larger positive inotropy in the mouse ventricle, where the functional role of Ca^{2+} extrusion through the forward mode NCX is larger. Ouabain treatment of the guinea-pig ventricle, which increases intracellular Na^+ concentration, would enhance Ca^{2+} influx from the reverse mode NCX. There is a report that inhibition of NCX by SEA0400 is more potent under higher intracellular Na^+ concentration (21). This may also partially underlie the difference in positive inotropy by SEA0400 between the guinea pig and mouse, which has a higher intracellular Na^+ concentration (22).

SEA0400 significantly reduced the ouabain-induced positive inotropy (Fig. 2), indicating that NCX activity is essential for ouabain action. Inhibition of inotropy induced by a higher concentration (3 μM) of ouabain was smaller (Fig. 5), probably because the inhibition of NCX is not complete (about 80%) with 1 μM SEA0400 (7). SEA0400 had no effect on IBMX-induced inotropy (Fig. 3), which reflects its high NCX specificity. Reduction of ouabain-induced inotropy by SEA0400 also suggests that the NCX is at least partly operating in the reverse mode in the presence of ouabain. Reduction of low-sodium contracture by SEA0400 indicated that it could inhibit Ca^{2+} influx through NCX not only in cardiomyocytes (7) but also in myocardial tissue. That ouabain can activate Ca^{2+} influx through reverse mode NCX was futher confirmed by induction of rise in intracellular Ca^{2+} concentration in HEK293 cells expressing the cardiac type NCX (Fig. 4). Thus, the present results provide pharmacological evidence for a contribution of the reverse mode NCX activity in the cardiac glycoside-induced inotropy. However, other mechanisms such as stimulation of sarcoplasmic reticulum (SR) Ca^{2+} release have also been postulated (23). The present results do not exclude such possibilities. Rather, inhibition of the NCX pathway by the highly specific inhibitor SEA0400 would be a useful strategy to clarify the additional mechanisms for cardiac glycoside-induced inotropy.

Ouabain has been considered to increase intracellular Na^+ concentration, shift the balance of the two modes of NCX to favor the reverse mode, and increase cellular Ca^{2+} load. When this Ca^{2+} load exceeds the capacity of the SR, abnormal Ca^{2+} release from the SR occurs, which in turn triggers abnormal electrical activity and arrhythmic contractions. In the present study, the ouabain-induced increase in basal tension and arrhythmic contractions were significantly reduced by SEA0400 (Fig. 5). This provides pharmacological evidence that NCX plays a crucial role in ouabain-induced arrhythmogenesis. It was also reported that SEA0400 attenuated ouabain-induced arrhythmia in a canine in vivo model (18) and in isolated Purkinje fibers (24). The effect of SEA0400 on other types of arrhythmia has also been investigated. Attenuation of arrhythmia induced by ischemia-reprefusion was shown to be attenuated by SEA0400 in the in vitro rat (13) and guinea-pig (16) model. On the other hand, SEA0400 was reported to be ineffective against various aconitine-induced arrhythmia models in the guinea pig (25). We have reported that KB-R7943, a less selective NCX inhibitor, inhibits aconitine-induced intracellular Ca^{2+} oscillations in isolated rat ventricular myocytes (26), which may reflect the action of KB-R7943 on ion channels other than the NCX (7).

In conclusion, the present results provide pharmaco-

logical evidence that the Na^+/Ca^{2+} exchanger is involved in ouabain-induced inotropy and arrhythmogenesis. SEA0400 may be promising as a therapeutic agent against arrhythmia dependent on NCX function.

Acknowledgments

This study was supported in part by a grant-in-aid for Drug Innovation Science Project to T.K. and K.S. from the Japan Health Science Foundation. This study was performed as a part of the project "Research on the molecular mechanisms of appearance of age-related diseases by failure of cell function control system, and their prevention and treatment" by the "Research Center for Aging and Age related Diseases" established in the Toho University Faculty of Pharmaceutical Sciences.

References

1 Bers D. Cardiac Na^+/Ca^{2+} exchange function in rabbit, mouse and man: what's the difference? J Mol Cell Cardiol. 2002;34:369–373.

2 Bers D. Cardiac myocytes Ca^{2+} and Na^+ regulation in normal and failing hearts. J Pharmacol Sci. 2006;100:315–322.

3 Maltsev VA, Vinogradova TM, Lakatta EG. The emergence of a general theory of the initiation and strength of the heartbeat. J Pharmacol Sci. 2006;100:338–369.

4 Levi A, Boyett M, Lee C. The cellular actions of digitalis glycosides on the heart. Prog Biophys Mol Biol. 1994;62:1–54.

5 Reuter H, Henderson S, Han T, Ross R, Goldhaber J, Philipson K. The Na^+-Ca^{2+} exchanger is essential for the action of cardiac glycosides. Circ Res. 2002;22:305–308.

6 Matsuda T, Arakawa N, Takuma K, Kishida Y, Kawasaki Y, Sakaue M, et al. SEA0400, a novel and selective inhibitor of the Na^+-Ca^{2+} exchanger, attenuates reperfusion injury in the in vitro and in vivo cerebral ischemic models. J Pharmacol Exp Ther. 2001;298:249–256.

7 Tanaka H, Nishimaru K, Aikawa T, Hirayama W, Tanaka Y, Shigenobu K. Effect of SEA0400, a novel inhibitor of sodium-calcium exchanger, on myocardial ionic currents. Br J Pharmacol. 2002;135:1096–1100.

8 Iwamoto T. Forefront of Na^+/Ca^{2+} exchanger studies: molecular pharmacology of Na^+/Ca^{2+} exchange inhibitors. J Pharmacol Sci. 2004;96:27–32.

9 Matsuda T, Koyama Y, Baba A. Functional proteins involved in regulation of intracellular Ca^{2+} for drug development: pharmacology of SEA0400, a specific inhibitor of the Na^+-Ca^{2+} exchanger. J Pharmacol Sci. 2005;97:339–343.

10 Namekata I, Kawanishi T, Iida-Tanaka N, Tanaka H, Shigenobu K. Quantitative fluorescence measurement of cardiac Na^+/Ca^{2+} exchanger inhibition by kinetic analysis in stably transfected HEK293 cells. J Pharmacol Sci. 2006;101:356–360.

11 Tanaka H, Namekata I, Takeda K, Kazama A, Shimizu Y, Moriwaki R, et al. Unique excitation-contraction characteristics of mouse myocardium as revealed by SEA0400, a specific inhibitor of Na^+/Ca^{2+} exchanger. Naunyn-Schmiedebergs Arch Pharmacol. 2005;371:526–534.

12 Ogata M, Iwamoto T, Tazawa N, Nishikawa M, Yamashita J, Takaoka M, et al. A novel and selective Na^+/Ca^{2+} exchange inhibitor, SEA0400, improves ischemia/reperfusion-induced renal injury. Eur J Pharmacol. 2003;478:187–198.

13 Takahashi K, Takahashi T, Suzuki T, Onishi M, Tanaka Y, Hamano-Takahashi A, et al. Protective effects of SEA0400, a novel and selective inhibitor of the Na^+/Ca^{2+} exchanger, on myocardial ischemia-reperfusion injuries. Eur J Pharmacol. 2003;458:155–162.

14 Magee W, Deshmukh G, Deninno M, Sutt J, Chapman J, Tracey W. Differing cardioprotective efficacy of the Na^+/Ca^{2+} exchanger inhibitors SEA0400 and KB-R7943. Am J Physiol Heart Circ Physiol. 2003;284:H903–H910.

15 Yoshiyama M, Nakamura Y, Omura T, Hayashi T, Takagi Y, Hasegawa T, et al. Cardioprotective effect of SEA0400, a selective inhibitor of the Na^+/Ca^{2+} exchanger, on myocardial ischemia-reperfusion injury in rats. J Pharmacol Sci. 2004;95: 196–202.

16 Namekata I, Nakamura H, Shimada H, Tanaka H, Shigenobu K. Cardioprotection without cardiosuppression by SEA0400, a novel inhibitor of Na^+-Ca^{2+} exchanger, during ischemia and reperfusion in guinea-pig myocardium. Life Sci. 2005;77:312–324.

17 Namekata I, Shimada H, Kawanishi T, Tanaka H, Shigenobu K. Reduction by SEA0400 of myocardial ischemia-induced cytoplasmic and mitochondrial Ca^{2+} overload. Eur J Pharmacol. 2006;543:108–115.

18 Nagasawa Y, Zhu B, Chen J, Kamiya K, Miyamoto S, Hashimoto K. Effects of SEA0400, a Na^+/Ca^{2+} exchange inhibitor, on ventricular arrhythmias in the in vivo dogs. Eur J Pharmacol. 2005;506:249–255.

19 Agata N, Tanaka H, Shigenobu K. Developmental changes in action potential properties of guinea-pig myocardium. Acta Physiol Scand. 1993;149:331–337.

20 Mukai M, Terada H, Sugiyama S, Satoh H, Hayashi H. Effects of a selective inhibitor of Na^+/Ca^{2+} exchange, KB-R7943, on reoxygenation-induced injuries in guinea pig papillary muscles. J Cardiovasc Pharmacol. 2000;35:121–128.

21 Lee C, Visen N, Dhalla N, Le H, Isaac M, Choptiany P, et al. Inhibitory profile of SEA0400 [2-[4-[(2,5-difluorophenyl) methoxy]phenoxy]-5-ethoxyaniline] assessed on the cardiac Na^+-Ca^{2+} exchanger, NCX1.1. J Pharmacol Exp Ther. 2004; 311:748–757.

22 Yao A, Su Z, Nonaka A, Zubair I, Lu L, Philipson KD, et al. Effects of overexpression of the Na^+-Ca^{2+} exchanger on $[Ca^{2+}]I$ transients in murine ventricular myocytes. Circ Res. 1998; 82:657–665.

23 Nishio M, Ruch S, Kelly J, Aistrup G, Sheehan K, Wasserstrom J. Ouabain increases sarcoplasmic reticulum calcium release in cardiac myocytes. J Pharmacol Exp Ther. 2003;308:1181–1190.

24 Nagy Z, Virag L, Toth A, Biliczki P, Acsai K, Banyasz T, et al. Selective inhibition of sodium-calcium exchanger by SEA-0400 decreases early and delayed after depolarization in canine heart. Br J Pharmacol. 2004;143:827–831.

25 Amran S, Hashimoto K, Homma N. Effects of sodium-calcium exchange inhibitors, KB-R7943 and SEA0400, on aconitine-induced arrhythmias in guinea pigs in vivo, in vitro, and in computer simulation studies. J Pharmacol Exp Ther. 2004;310: 83–89.

26 Namekata I, Yamagishi R, Kato Y, Nakamura R, Tanaka H, Shigenobu K. Propagation of normal and abnormal cytoplasmic Ca^{2+} oscillation into the cell nucleus in cardiomyocytes. Bioimages. 2004;12:61–69.

ARTICLE IN PRESS
MODEL 5
Available online at www.sciencedirect.com
ScienceDirect
ELSEVIER
Biologicals xx (2007) 1–11
BIOLOGICALS
www.elsevier.com/locate/biologicals

Influences of the recombinant artificial cell adhesive proteins on the behavior of human umbilical vein endothelial cells in serum-free culture

Akiko Ishii-Watabe [a,*], Toshie Kanayasu-Toyoda [b], Takuo Suzuki [a], Tetsu Kobayashi [a], Teruhide Yamaguchi [b], Toru Kawanishi [a]

[a] *Division of Biological Chemistry and Biologicals, National Institute of Health Sciences, 1-18-1 Kamiyoga, Setagaya-ku, Tokyo 158-8501, Japan*
[b] *Division of Cellular and Gene Therapy Products, National Institute of Health Sciences, 1-18-1 Kamiyoga, Setagaya-ku, Tokyo 158-8501, Japan*

Received 8 June 2006; revised 4 December 2006; accepted 22 December 2006

Abstract

To improve the safety of cellular therapy products, it is necessary to establish a serum-free cell culture method that can exclude animal-derived materials in order to avoid contamination with transmissible agents. It would be optimal if the proteins necessary to a serum-free culture could be provided as recombinant proteins. In this study, the influences of recombinant artificial cell adhesive proteins on the behavior of human umbilical vein endothelial cells (HUVECs) in serum-free culture were examined in comparison with the influence of plasma fibronectin (FN). The recombinant proteins used were Pronectin F (PF), Pronectin F PLUS (PFP), Pronectin L (PL), Retronectin (RN), and Attachin (AN). HUVECs adhered more efficiently on PF or PFP than on FN. No cells adhered on PL. Regarding the VEGF or bFGF-induced cell growth, the cells on PF and PFP proliferated at a similar rate to the cells on FN. RN and AN were less effective in supporting cell growth. Since cell adhesion on PF and PFP induced phosphorylation of focal adhesion kinase, they are thought to activate integrin-mediated intracellular signaling. The cells cultured on PF or PFP were able to produce prostaglandin I_2 or tissue-plasminogen activator in response to thrombin. However, thrombin caused detachment of the cells from PF but not from PFP or FN, meaning that the cells were able to adhere more tightly on PFP or FN than on PF. These data indicate that PFP could be applicable as a substitute for plasma FN.

Keywords: Cell adhesive protein; Recombinant protein; Fibronectin; Endothelial cells

1. Introduction

The widespread development of cellular therapy products has advanced to the stage of non-clinical and clinical testing [1–3]. Regulatory documents for human somatic cell therapy including instructions for investigational new drug applications have been published [4–6]. To guarantee the safety of both product recipients and the public at large, it is crucial to prevent contamination of cellular therapy products by infectious agents [7].

Serum-free culture is one of the desired methods for manufacturing cellular therapy products when safety issues are a concern [8,9]. Although serum is a very effective additive for a culture medium that can support cell adhesion, survival, growth, and functions, animal-derived materials such as serum may contain transmissible agents or human allergens [10–13]. Since serum is composed of proteins, sugars, lipids, vitamins, and other ingredients, its quality is affected by the genetic and environmental circumstances of the animal used, which means there are lot-to-lot variations in composition and potency. This variability could reduce the consistency of cellular therapy products, and a serum-free culture that could contribute to improving the consistency of the cell features is thus needed.

Protein factors often need to be added to serum-free culture to substitute for the functions of serum. The proteins used for this purpose must also pose no risk of infection. Because recombinant proteins can be produced without using animal-derived materials, and pose little risk of contaminating human pathogens, they are a useful biomaterial for culturing cells

* Corresponding author. Tel./fax: +81 3 3700 9084.
E-mail address: watabe@nihs.go.jp (A. Ishii-Watabe).

1045-1056/07/$32.00 © 2007 The International Association for Biologicals. Published by Elsevier Ltd. All rights reserved.
doi:10.1016/j.biologicals.2006.12.002

Please cite this article in press as: Ishii-Watabe A. et al., Influences of the recombinant artificial cell adhesive proteins on the behavior of human umbilical vein endothelial cells in serum-free culture, Biologicals (2007), doi:10.1016/j.biologicals.2006.12.002

when safety issues are a concern. In addition, the functions of recombinant proteins can be improved by modifying their amino acid sequences, which is also an advantage. In this study, using a serum-free culture of human umbilical vein endothelial cells (HUVECs), the usefulness of recombinant artificial cell adhesive proteins as a plasma fibronectin substitute was evaluated.

The extracellular matrix glycoprotein fibronectin consists of two similar polypeptide chains, each with a molecular mass of approximately 250 kDa joined at their respective C termini by disulfide bonds [14,15]. The RGD (arginine–glycine–aspartic acid) recognition sequence located within the molecule was the first amino acid motif shown to mediate cell adhesion [16,17]. Intracellular signaling induced by cell adhesion on fibronectin plays a critical role in cytoskeletal reorganization, cell cycle progression, and cell survival [18,19].

This study defines the influences of five different kinds of recombinant artificial cell adhesive proteins on endothelial adhesion, proliferation, and antithrombotic function in serum-free culture for which plasma fibronectin is needed. The recombinant proteins used were Pronectin F, Pronectin F PLUS, Pronectin L, Retronectin, and Attachin (Table 1).

2. Materials and methods

2.1. Recombinant cell adhesive proteins

Pronectin F, Pronectin F PLUS, and Pronectin L were purchased from Sanyo Chemical Industry (Kyoto, Japan), Retronectin from TaKaRa (Shiga, Japan), and Attachin from Bio999 (Taipei, Taiwan). All of these proteins were produced via bacterial fermentation. Pronectin F is a genetically engineered protein containing repeating units of the RGD sequence interspersed with a β-silk peptide for structural stability [20]. It is comprised of 980 amino acids. Based on its sequence, the molecular weight is estimated to be 72,728. The amino acid sequence is fMDPVVLQRRDWENPGVTQLNRLAA HPPFASDPMGAGS(GAGAGS)$_6$GAAVTGRGDSPASAAGY-[(GAGAGS)$_9$GAAVTGRGDSPASAAGY]$_{12}$-(GAGAGS)$_2$GA GAMDPGRYQLSAGRYHYQLVWCQK. Pronectin F PLUS is a positively charged water-soluble variant of Pronectin F that is produced by chemical modification [21,22]. Pronectin L is a protein polymer that exhibits IKVAV epitopes from the laminin alpha chain with a similar backbone as Pronectin F [21]. It is comprised of 1019 amino acids. The molecular weight is estimated to be 75,639. The amino acid sequence is fMDPVVLQRRDWENPGVTQLNRLAAHPPFASDPMGA GS(GAGAGS)$_6$GAAPGASIKVAVSAGPSAGY-[(GAGAGS)$_9$ GAAPGAIKVAVSAGPSAGY]$_{12}$-(GAGAGS)$_2$GAGAMDPG RYQLSAGRYHYQLVWCQK. Retronectin consists of a central cell-binding domain, a high affinity heparin-binding domain II, and a CS1 site within an alternatively spliced type III connecting segment region of human fibronectin [23]. It is comprised of 574 amino acids. The molecular weight is estimated to be 62,631. Attachin is an artificial fusion protein with the molecular weight of 30 kDa that has several functional domains, including a fibronectin-like cell attachment domain [24]. It has reportedly been used to promote the adhesion of several kinds of cell lines, including CHO-K1, MDBK, PK-15, L929, Vero, COS, U373, Swiss 3T3, and MRC-5 [25].

2.2. Cells and materials

Human umbilical vein endothelial cells (HUVECs) were purchased from Sanko Junyaku (Tokyo, Japan) and maintained

Table 1
Fibronectin and recombinant cell adhesive proteins used in this study

Proteins	Structure	Molecular Weight
Fibronectin	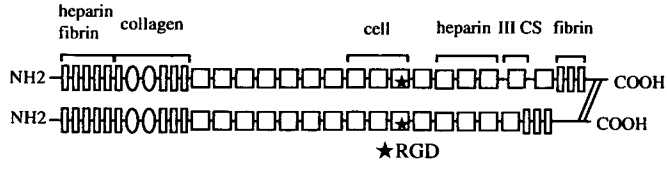	250K x 2
Pronectin F	Head-[(GAGAGS)9GAAVTGRGDSPASAAGY]12-Tail ★	73K
Pronectin F Plus	Positively charged, water-soluble variant of Pronectin F	73K
Pronectin L	Head-[(GAGAGS)9GAAPGASIKVAVSAGPSAGY]12-Tail ◆	76K
Retronectin	Chimeric protein of human fibronectin fragment 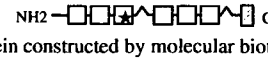	63K
Attachin	A fusion protein constructed by molecular biotechnology	30K

Fibronectin.
▯ Type I module.
0 Type II module.
□ Type III module.
★: cell attachment sequence derived from fibronectin.
◆: cell attachment sequence derived from laminin.

Please cite this article in press as: Ishii-Watabe A et al., Influences of the recombinant artificial cell adhesive proteins on the behavior of human umbilical vein endothelial cells in serum-free culture, Biologicals (2007), doi:10.1016/j.biologicals.2006.12.002

in EGM-2 media (Cambrex, Walkersville, MD) on collagen-coated dishes (Asahi Techno Glass, Tokyo, Japan). EGM-2 media is modified MCDB 131 containing 2% fetal bovine serum, VEGF, bFGF, IGF-1, EGF, heparin, hydrocortisone and ascorbic acid. The cells were kept in a humidified, 5% CO_2 environment at 37 °C. Cells between passages 3 and 5 were used for all experiments.

The serum-free media used was human endothelial SFM (Invitrogen, Carlsbad, CA) [26]. Ten nanograms/ml of epidermal growth factor (EGF) (Invitrogen) and 20 ng/ml of basic fibroblast growth factor (bFGF) (Invitrogen) were added as supplements. Fibronectin is recommended for use as a cell attachment factor.

2.3. Cell adhesion assay

Recombinant cell adhesive proteins were diluted with phosphate buffered saline (PBS(−)), and plated on multiwell non-treated polystyrene plates (BD Falcon, Franklin Lakes, NJ). The plates were incubated for 2 h at room temperature, and then the protein solutions were removed and the wells washed with PBS(−). The concentration of the recombinant proteins used was 10 μg/ml (2 μg/cm^2), unless the description states otherwise. The amount of absorbed protein was quantified with a QuantiPro BCA Kit (Sigma, St. Louis, MO) using bovine serum albumin as a standard.

The HUVECs were harvested using trypsin and washed twice with PBS(−). The cells were then suspended in serum-free media, and added to each well of 96-well plates previously coated with recombinant cell adhesion proteins at a cell density of 1×10^4 cells/well. After incubating for 60 min under 5% CO_2 at 37 °C, the supernatant was removed, and the wells rinsed with PBS(−) to remove non-adherent cells. Following fixation of the adherent cells by 4% paraformaldehyde for 10 min, the paraformaldehyde was removed and the cells washed once with distilled water. A 0.5% (w/v) solution of crystal violet was then added to the wells. After staining for 25 min, the cells were rinsed five times with distilled water and the crystal violet that was absorbed on the adherent cells was solubilized with 0.5% SDS. The optical density at 595 nm was measured on an EL340 plate reader (BioTek Instruments, Winooski, VT).

2.4. Measurement of cell proliferation

HUVECs were harvested and suspended in serum free media, and plated to each well of the 96-well plates previously coated with recombinant cell adhesive proteins. VEGF (R&D Systems, Minneapolis, MN) or bFGF (Invitrogen, Carlsbad, CA) was added at concentrations of 1−100 ng/ml. After culturing for 2 days under 5% CO_2 at 37 °C, the cell number in each well was measured using Cell Counting Kit-8 (Dojindo, Kumamoto, Japan). Results are expressed as the mean value ± S.D. of triplicate determinations.

2.5. Phosphorylation of focal adhesion kinase

The HUVECs were collected by trypsin treatment (Invitrogen), resuspended in serum free medium, incubated for 2 h at 37 °C in suspension, and subsequently plated at 5×10^5 cells/dish on 60 mm diameter dishes pre-coated with cell adhesive proteins or bovine serum albumin (BSA) (10 μg/ml) [27]. After incubation for 2 h under 5% CO_2 at 37 °C, the cells were lysed in RIPA buffer (50 mM Tris−HCl (pH 7.6), 150 mM NaCl, 1% NP-40, 0.25% sodium deoxycholate), and the protein concentrations were determined using the BCA assay (Pierce, Rockford, IL). 3.5 μg of the total cell lysates was resolved by SDS−PAGE, blotted onto Immobilon-P membranes (Millipore, Volketswil, Switzerland), and incubated in 1% BSA with anti-pY397 FAK antibody (Upstate Biotechnology Inc.,, Lake Placid, NY) followed by incubation with horseradish peroxidase-labeled secondary antibody (Cell Signaling Technology, Danvers, MA). The ECL system (GE Healthcare Bio-Sciences AB, Uppsala, Sweden) and Luminoimage analyzer LAS 3000 (Fuji Film, Kanagawa, Japan) were used for detection. The membranes were stripped of bound antibody using a Re-Blot Plus Western Blot Recycling Kit (Chemicon, Temecula, CA), and the membrane was reprobed with anti-FAK antibody (Upstate Biotechnology). The labeled bands were quantified using the MultiGauge software program (Science Lab). The quantified value for phosphorylated FAK was normalized with that for total FAK in each sample, and the relative phosphorylation level was then calculated as a ratio against the cell lysate on fibronectin.

2.6. Secretion of Prostaglandin I_2 (PGI_2)

The HUVECs were harvested using trypsin, washed twice, and then suspended in serum-free media. The cells were placed on the 24-well plates coated with recombinant cell adhesive proteins at the density of 7×10^4/well. After culturing for 1 day, the cells were stimulated with 1 U/ml of thrombin or 30 ng/ml of VEGF. The cells were incubated for 1 h under 5% CO_2 at 37 °C, and then the supernatant was collected. The supernatant was centrifuged for 10 min at 2000 × g in a microcentrifuge to remove any residual cells. The level of 6-keto Prostaglandin $F_1\alpha$, a major metabolite of Prostaglandin I_2, was determined using 6-keto Prostaglandin $F_1\alpha$ EIA Kit (Cayman Chemical, Ann Arbor, MI). Each culture condition was repeated in triplicate.

2.7. Secretion of tissue-plasminogen activator

The HUVECs were seeded as described above. After culturing for 1 day, the cells were stimulated with 0.01−1 U/ml of thrombin. Twenty-four hours later, the supernatant was collected and spun down for 10 min at 2000 × g in a microcentrifuge. The level of tissue plasminogen activator was determined using the AssayMax Human Tissue-Type Plasminogen Activator ELISA Kit (Assay Pro, Brooklyn, NY). Each culture condition was repeated in triplicate. Phase contrast images were obtained before the supernatant was collected.

Please cite this article in press as: Ishii-Watabe A et al., Influences of the recombinant artificial cell adhesive proteins on the behavior of human umbilical vein endothelial cells in serum-free culture, Biologicals (2007), doi:10.1016/j.biologicals.2006.12.002

3. Results

3.1. Adhesion of HUVECs onto recombinant cell adhesive proteins

To examine the adhesion onto the recombinant cell adhesive proteins, HUVECs harvested and suspended in serum-free media were applied on plastic wells precoated with Pronectin F, Pronectin F PLUS, Pronectin L, Retronectin, Attachin, or fibronectin (Table 1). As shown in Fig. 1, Pronectin F, Pronectin F PLUS, Retronectin, or Attachin showed cell adhesion activity to a similar extent as fibronectin at the concentration of 10 μg/ml (2 μg/cm^2). Pronectin F and Pronectin F PLUS were superior to fibronectin when they were used at an amount of less than 1 μg/ml. The cells were observed under microscopy to have spread well on the recombinant proteins that they adhered to (Fig. 2). No cells had adhered onto Pronectin L or BSA.

In order to test if these differences are due to the difference in the absorbed amount of each protein, the protein absorbed on the plate was measured (Fig. 3). It was found that Pronectin F and Pronectin L had absorbed to the plate better than other proteins and that the absorbed amount of Pronectin F PLUS was lower than that of Pronectin F and Pronectin L. From the point of view of the efficiency of cell adhesion (Fig. 1) and the absorbed amount of protein (Fig. 3), the number of cells attached was not dependent on the amount of absorbed protein, suggesting that the observed effects were not due to differences in protein absorption but rather due to the character of each cell adhesion protein.

3.2. Influences on cell proliferation

Besides anchorage, cell adhesion to components of the extracellular matrix triggers signaling events affecting diverse cellular traits and activities, including survival, proliferation, and other functions. Therefore, the influences of the recombinant cell adhesion proteins on cell proliferation were examined. The HUVECs in serum-free media were seeded on the plates that were coated with recombinant cell adhesive proteins, and then cultured in the presence or absence of basic fibroblast growth factor (bFGF) or vascular endothelial growth factor (VEGF) at concentrations from 1 to 100 ng/ml. After culturing for 2 days, the cell numbers in each well were examined (Fig. 4). When HUVECs were cultured in the presence of bFGF, the cells on Pronectin F or Pronectin F PLUS had grown to the same level as that on fibronectin in each concentration of bFGF, showing that Pronectin F and Pronectin F PLUS have the same growth support potency as fibronectin (Fig. 4A). However, the cell numbers on Retronectin or Attachin reached 70% or 40% of that on fibronectin, respectively; showing that the growth support potency of Retronectin and Attachin was lower than fibronectin. When VEGF-stimulated cell proliferation was examined, Pronectin F and Pronectin F PLUS also showed similar growth-supporting potency to fibronectin (Fig. 4B). Retronectin and Attachin were less effective than fibronectin.

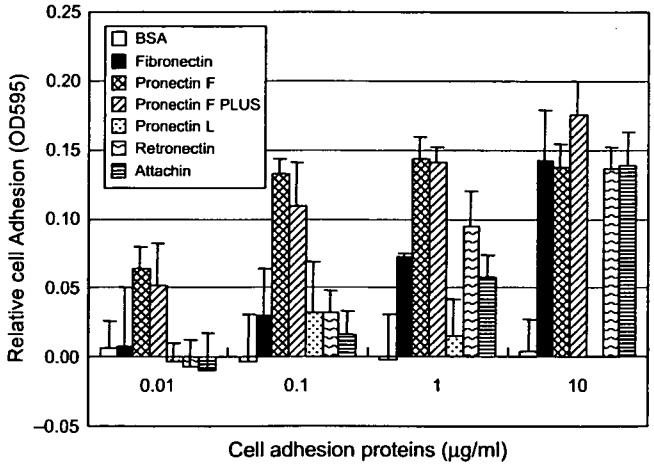

Fig. 1. Adhesion of HUVECs to recombinant cell adhesive proteins. HUVECs were plated into wells previously coated with Fibronectin, Pronectin F, Pronectin F PLUS, Pronectin L, Retronectin, Attachin, or BSA, and then incubated for 1 h at 37 °C. Attached cells were fixed and stained with crystal violet and quantified by absorbance reading. Results are expressed as mean value ± S.D. of triplicate determinations. The 0.1 OD corresponded to 0.61 ± 0.085 × 10^4 cells.

3.3. Phosphorylation of focal adhesion kinase

Cell adhesive proteins activate intracellular signaling via cell surface integrins. In regulating the cellular responses to integrin-mediated adhesion, focal adhesion kinase (FAK) has emerged as a key signaling molecule [28–30]. Integrin–ligand engagement promotes FAK tyrosine phosphorylation that promotes FAK signaling activity. The phosphorylation of FAK Tyr-397, the only apparent autophosphorylation site, is known to create a high-affinity binding site for SH2 domains of the Src-family kinases, including c-Src and Fyn [31].

HUVECs cultured in growing media were harvested by trypsin treatment, and incubated in serum-free media for 2 h at 37 °C in suspension. After this incubation, the cells were plated onto the dishes in which recombinant cell adhesive proteins were coated, and then incubated for 2 h under 5% CO_2 at 37 °C. Cell lysates were prepared using RIPA buffer, and the phosphorylation level of FAK on Tyr 397 was then examined by Western blotting. As shown in Fig. 5, FAK Tyr-397 is phosphorylated under an attached condition (lane 1), becomes dephosphorylated upon cell suspension (lane 2), and then becomes rephosphorylated after replating. The FAK phosphorylation level after replating on recombinant proteins differed in each sample (lanes 3–10). Phosphorylation level of cells on BSA (lane 3) or Pronectin L (lane 7), to which cells did not adhere, was still lower after replating. Pronectin F (lane 5) or Pronectin F PLUS (lane 6) induced FAK phosphorylation to the similar extent to Fibronectin (lane 4), suggesting that Pronectin F and Pronectin F PLUS are thought to activate intracellular signaling via integrin as well as fibronectin. Retronectin that has RGD domain of Fibronectin also induced FAK phosphorylation (lane 8).

Please cite this article in press as: Ishii-Watabe A et al., Influences of the recombinant artificial cell adhesive proteins on the behavior of human umbilical vein endothelial cells in serum-free culture, Biologicals (2007), doi:10.1016/j.biologicals.2006.12.002

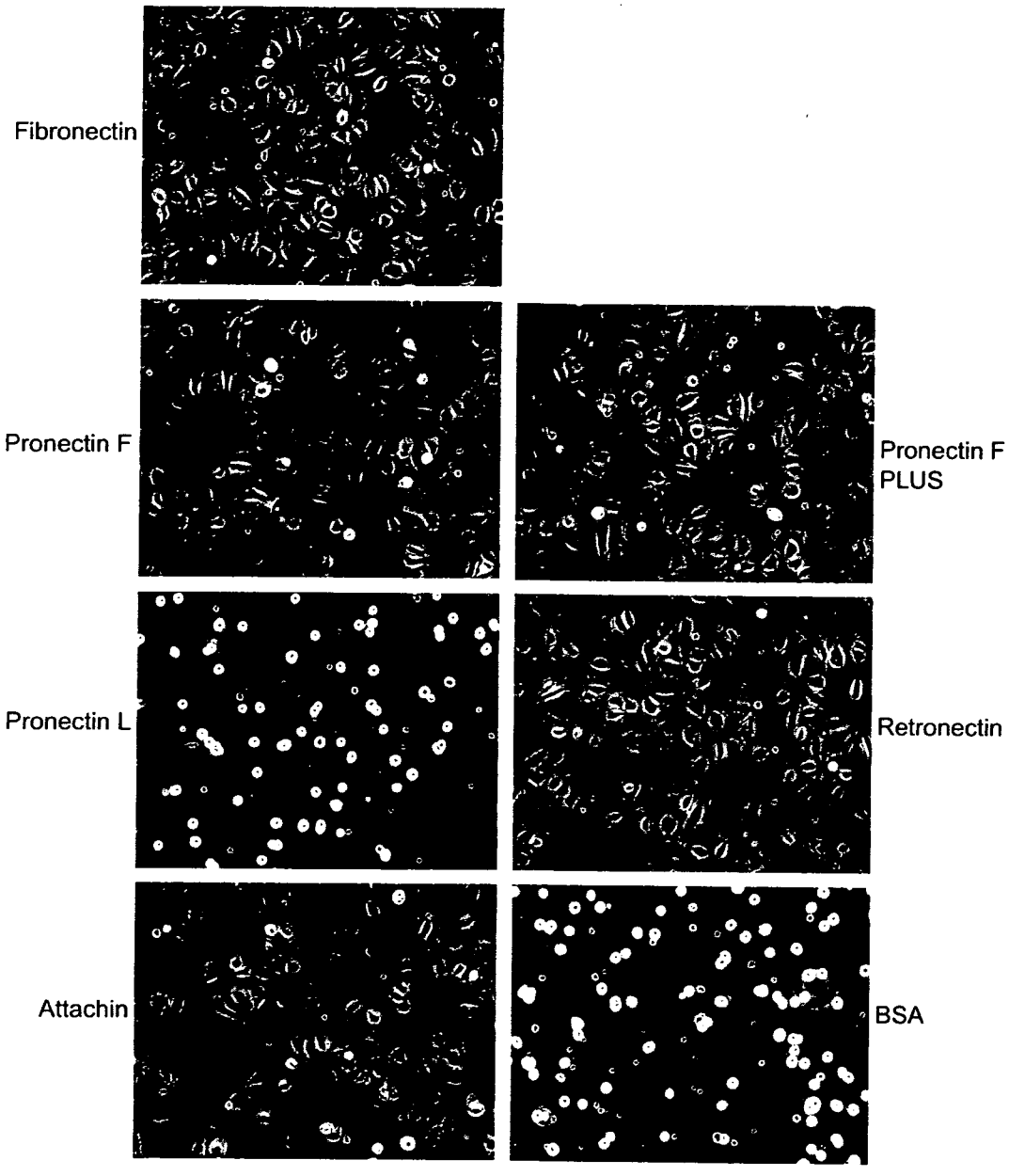

Fig. 2. The phase contrast images of cell attachment and spreading on recombinant cell adhesive proteins. HUVECs were seeded into wells previously coated with 10 μg/ml of Fibronectin, Pronectin F, Pronectin F PLUS, Pronectin L, Retronectin, Attachin, or BSA. After 1 h incubation at 37 °C, the cells were photographed with an inverted microscope.

3.4. Influences on antithrombotic functions of endothelial cells

In order to examine the influences of recombinant cell adhesive proteins on cellular functions, the production of prostaglandin I_2 (PGI_2) and tissue-plasminogen activator (t-PA), both of which play important roles in the antithrombotic feature of endothelial cells, was tested. Antithrombotic activity is the most important characteristic of endothelial cells that are used for artificial blood vessels or engineered vascularized tissues. PGI_2 inhibits platelet aggregation, thereby inhibiting the formation of thrombus. It is produced quickly after stimulation via the activation of phospholipase A_2. Since the half life of PGI_2 is as short as 2 min, the concentrations of its metabolite 6-keto Prostaglandin $F_1\alpha$ were measured. t-PA is produced from endothelial cells via the induction of protein synthesis in response to the extracellular stimuli. It induces the processing of plasminogen to plasmin, and dissolves the fibrin clots.

HUVECs were plated on the recombinant cell adhesion protein-coated dishes and cultured for 1 day, then stimulated with VEGF or thrombin. As shown in Fig. 6A, PGI_2 was produced from VEGF- stimulated HUVECs on different kinds of cell adhesive proteins to the same level. In the serum-free media, the basal production of PGI_2 was higher, and the production after the stimulation was less than in the growing

Please cite this article in press as: Ishii-Watabe A et al., Influences of the recombinant artificial cell adhesive proteins on the behavior of human umbilical vein endothelial cells in serum-free culture, Biologicals (2007), doi:10.1016/j.biologicals.2006.12.002